AO4ELT7 - June 2023 - Avignon

Marginalized semi-blind restoration of Adaptive-Optics-corrected images using stochastic sampling

Alix Yan[a,*], Laurent M. Mugnier[a], Jean-François Giovannelli[b], Romain Fétick[a], and Cyril Petit[a]

[a]DOTA/ONERA - Université Paris Saclay, 29 Avenue de la Division Leclerc, Châtillon, France
[b]IMS (Univ. Bordeaux, CNRS, BINP), 351 Cours de la Libération, Talence, France

ABSTRACT

Adaptive optics (AO) corrected image restoration is particularly difficult, as it suffers from the lack of knowledge on the point spread function (PSF) in addition to usual difficulties. An efficient approach is to marginalize the object out of the problem and to estimate the PSF and (object and noise) hyperparameters only, before deconvolving the object using these estimates. Recent works have applied this marginal semi-blind deconvolution method, based on the Maximum A Posterior (MAP) estimator, combined to a parametric model of the PSF, to a series of AO corrected astronomical and satellite images. However, this method does not enable one to infer global uncertainties on the estimated parameters, nor to compute posterior correlations between the sought parameters.

In this communication, we propose to use a new restoration method that allows to infer such uncertainties (Yan et al., JATIS, to appear, 2023). This method consists in choosing the Minimum Mean Square Error (MMSE) estimator and computing the latter as well as the associated uncertainties thanks to a Markov chain Monte Carlo (MCMC) algorithm.

We validate our method by means of realistic simulations in the context of an astronomical observation. Finally, we present results on an experimental image of asteroid Vesta, taken on VLT/SPHERE with the Zimpol instrument.

Keywords: Image restoration, semi-blind deconvolution, adaptive optics, astronomical imaging, satellite imaging, MCMC, Bayes

1. INTRODUCTION

Ground-based high angular resolution imaging in the visible has numerous applications in astronomy, such as the observation of asteroids. The observations are limited by atmospheric turbulence, which can be corrected in real time by adaptive optics (AO). However, the correction is partial and residual blurring remains, impacting high

Further author information: Send correspondence to L.M.M. E-mail: mugnier at onera.fr

spatial frequencies of the observed object. Therefore, the observation system includes post-processing to restore the high frequencies.

The residual blurring is described by the system point-spread function (PSF), which is not entirely known, so both the observed object and the PSF are estimated. A way to proceed is to first estimate the PSF by "marginalizing" over the object, *i.e.* by integrating the joint probability density function over all possible objects with a given prior probability density function, and then to deconvolve the image with the estimated PSF.[1] In our case, the PSF has a physical parametric model and the object is described by a Gaussian prior with a parametric model for its power spectral density (PSD), whose parameters are also estimated along with PSF parameters. The method we have been using so far, AMIRAL (standing for Automatic Myopic Image Restoration ALgorithm), combines PSF and PSD parametrization as well as a marginal maximum *a posteriori* (MAP) estimator.[2]

The method we propose in the present paper uses another Bayesian estimator, which minimizes the mean square error on the sought parameters (MMSE estimator), corresponding to the mean of the marginal posterior distribution. From this method, we also infer uncertainties on PSF and PSD parameters[3] and compute posterior correlations between them. To do so, we include prior distributions for PSF and PSD parameters and we compute the marginal posterior distribution by stochastic sampling. We first introduce our framework, as well as a Markov chain Monte Carlo (MCMC) algorithm to sample this posterior distribution: this method is further detailed in [4]. Then, we validate our method on simulated astronomical data and we finally apply it to experimental astronomical data.

2. IMAGING MODEL AND MMSE ESTIMATOR

2.1 Imaging equation

We consider that the image $\boldsymbol{i}$ results from the 2D discrete convolution of the object $\boldsymbol{o}$ with the PSF $\boldsymbol{h}$, to which noise $\boldsymbol{n}$ (mostly photon noise and detector readout noise) is added, giving the following imaging model:

$$\boldsymbol{i} = \boldsymbol{h} * \boldsymbol{o} + \boldsymbol{n}. \tag{1}$$

In this study, we simulate and restore astronomical AO-corrected images taken on a VLT/SPHERE-like instrument[5] with the Zimpol imaging polarimeter.[2]

Throughout this work, we will consider having long-exposure PSFs, meaning that the exposure time is greater than the typical variation time of turbulence. For the PSF, we use the PSFAO19 model,[6] which has been designed specifically for describing an AO-corrected PSF with few physical parameters. The two main parameters of the PSFAO19 model, are the Fried parameter r_0 taken at the imaging wavelength (850 nm), describing the turbulence's strength, and the variance of the residual turbulent phase v_ϕ, describing the quality of AO correction. In this study, the AO parameters as well as other PSF secondary parameters are taken identical to those in,[2] for comparison purposes.

2.2 Prior distributions

Noise is taken independently from the object, and is approximated as zero-mean, additive, white and Gaussian, which is a fine description given the flux levels in typical images. We denote the noise precision (inverse variance) by γ_n, thus the noise covariance matrix is $\boldsymbol{R_n} = 1/\gamma_n \boldsymbol{I}$, with $\boldsymbol{I}$ the identity matrix and the noise PSD is $S_n = 1/\gamma_n$.

An example of simulated astronomical observation is given in Figure 1, with the true object on the left and the simulated image on the right. The image is simulated using the PSFAO19 model.

As a prior for the object, we consider a Gaussian model described by its mean $\boldsymbol{m}_o$ and its PSD $\boldsymbol{S}_o$. Given that we have little information on the the mean object $\boldsymbol{m}_o$, it is taken uniform on all pixels, estimated at the average value of the image considering that $\sum \boldsymbol{h} = 1$, modeling flux conservation. For the object PSD, we use the following parametric model:

$$S_o(\boldsymbol{f}) = \frac{1}{\gamma_o} \bar{S}_o(\boldsymbol{f}), \text{ with } \bar{S}_o(\boldsymbol{f}) = 1/(k + f^p), \tag{2}$$

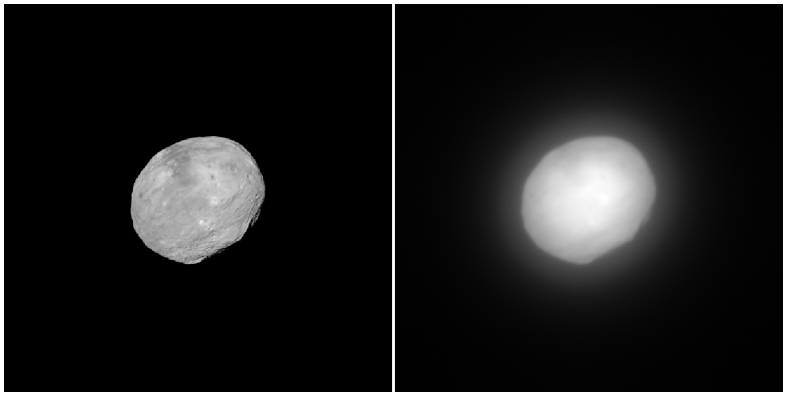

Figure 1. Left: synthetic view of Vesta (true object $\boldsymbol{o}$), of size 512×512. Right: simulated image $\boldsymbol{i}$, with true parameters $r_0 = 0.15\,\mathrm{m}$, $v_\phi = 1.3\,\mathrm{rad}^2$ and $\gamma_n = 2.62\ 10^{-4}\,\mathrm{ph}^{-2}$.

and $f = |\boldsymbol{f}|$ the radial frequency. This circularly-symmetric model is a slightly modified writing of Matérn's model.[7] In this model, γ_o sets the global PSD level, p is the PSD decrease rate at high frequencies, and k gives the breakpoint between the two regimes of the model. In previous works,[2] attempts to estimate hyperparameter p jointly with the other parameters has been shown to strongly decrease PSF parameter estimation accuracy. Therefore, we choose to work in a "mostly unsupervised" mode, where p is fixed to a standard value. In the case of astronomical observations of asteroids, a well-fitting empirical value is around $p = 3$.

Regarding PSF parameters as well as noise and object PSD parameters, hereafter called parameters, we use uniform priors for each parameter γ_n, γ_o, k, r_0 and v_ϕ. In our model, we assume that the image $\boldsymbol{i}$ and object PSD parameters γ_o and k are independent conditionally to the object and the other parameters. Additionally, the object, the noise variance and the PSF parameters are taken independent conditionally to object PSD parameters. Moreover, the parameters (γ_o, k, r_0, v_ϕ and γ_n) are modeled as *a priori* independent.

2.3 Marginal estimator

The expression of the marginal posterior distribution is calculated from the integration of the joint distribution over the object. This joint distribution is itself, following the conditioning rule, the multiplication of the likelihood by the prior distributions. In practice, we write the marginal posterior distribution following the Bayes rule, from the marginal likelihood and the priors taken as uniform and independent, as mentioned in section 2.2:

$$p(\gamma_n, \gamma_o, k, r_0, v_\phi|\boldsymbol{i}) = \frac{p(\gamma_n)p(\gamma_o)p(k)p(r_0)p(v_\phi)}{p(\boldsymbol{i})} p(\boldsymbol{i}|\gamma_n, \gamma_o, k, r_0, v_\phi). \tag{3}$$

Given that the noise is taken Gaussian, white and *a priori* independent from the object considered Gaussian, the image being a linear combination of both is also Gaussian. Therefore, the marginal likelihood writes:

$$p(\boldsymbol{i}|\gamma_n, \gamma_o, k, r_0, v_\phi) = (2\pi)^{-P/2} \prod_{\boldsymbol{f}} \Big(S_i(\boldsymbol{f})^{-1/2} \exp\big[-\frac{1}{2} |\tilde{i}(\boldsymbol{f}) - \tilde{m}_i(\boldsymbol{f})|^2 / S_i(\boldsymbol{f}) \big] \Big), \tag{4}$$

with image PSD $\boldsymbol{S}_i$ and mean image $\boldsymbol{m}_i$:

$$\begin{aligned} S_i(\boldsymbol{f}) &= S_o(\boldsymbol{f}) |\tilde{h}(\boldsymbol{f})|^2 + S_n \\ \tilde{m}_i(\boldsymbol{f}) &= \tilde{h}(\boldsymbol{f}) \tilde{m}_o(\boldsymbol{f}). \end{aligned} \tag{5}$$

2.4 MMSE estimator and sampling

Given the complexity of the marginal posterior distribution, there is no known analytical way to calculate it. A way to compute it is to draw samples under the posterior distribution using a MCMC method for instance, and compute the sample mean. The posterior distribution being complex, it is not possible to sample it directly,

therefore we use a Metropolis-Hastings algorithm to bypass the problem.[8] It consists, for each iteration, in drawing samples under a chosen proposal distribution and accepting the samples (else, duplicating the previous value) with a prescribed probability. For simplicity, we use here the Metropolis-Hastings algorithm within a Gibbs algorithm, in order to draw under its own conditional posterior distribution, which is proportional to the prior of the considered parameter times the marginal likelihood of Eq. (4). Asymptotically, the samples are under the marginal posterior distribution for all parameters, and the samples average tends towards the mean of the distribution.[8] A typical number of iterations needed to reach convergence would be around 30 000 iterations, corresponding to an hour on an ordinary laptop. This method is further explained in [4].

3. RESULTS ON SIMULATED ASTRONOMICAL DATA

3.1 Simulation conditions

The obtained results are shown for the simulated image displayed in Figure 1, using as the true object the synthetic view of asteroid Vesta, built by the OASIS software,[9] on a dark background of size 512×512 pixels. True PSF parameters are $r_0 = 0.15\,\mathrm{m}$ and $v_\phi = 1.3\,\mathrm{rad}^2$ at the imaging wavelength $\lambda = 550\,\mathrm{nm}$, which correspond to realistic turbulence and correction conditions. The AO system is a "SPHERE-like" AO system, and its parameters are taken identical to those used with the previous method,[2] for comparison purposes. Noise is taken zero-mean, additive, white and Gaussian with a variance equal to the empirical mean value of the object as a first approximation of the photon noise. The total flux of the object is set to $F_o = 10^9\,\mathrm{ph}$ (photons), typical from VLT/SPHERE/Zimpol asteroid observations (ESO Large Program ID 199.C-0074), therefore $\gamma_n = P/F_o = 2.62 \times 10^{-4}\,\mathrm{ph}^{-2}$.

The PSF and PSD parameters are estimated following the proposed method, except the mean object $\boldsymbol{m}_o$, which is estimated to the average value of the image, and the object PSD power which is fixed to $p = 3$, which corresponds to a reasonable default value of p for asteroids. The Gibbs sampler is run for 100 000 iterations, which corresponds to a few hours, to verify the convergence.

3.2 Results on the estimated parameters and derived uncertainties

In Figure 2, we plot the samples chains and the corresponding histograms for γ_n, r_0 and v_ϕ. The inspection of Figure 2 suggests that chains have a short burn-in period, followed by a stationary state. As expected from Markov chains, for each parameter the samples are correlated. Moreover, the samples are concentrated in a small interval relatively to their prior interval.

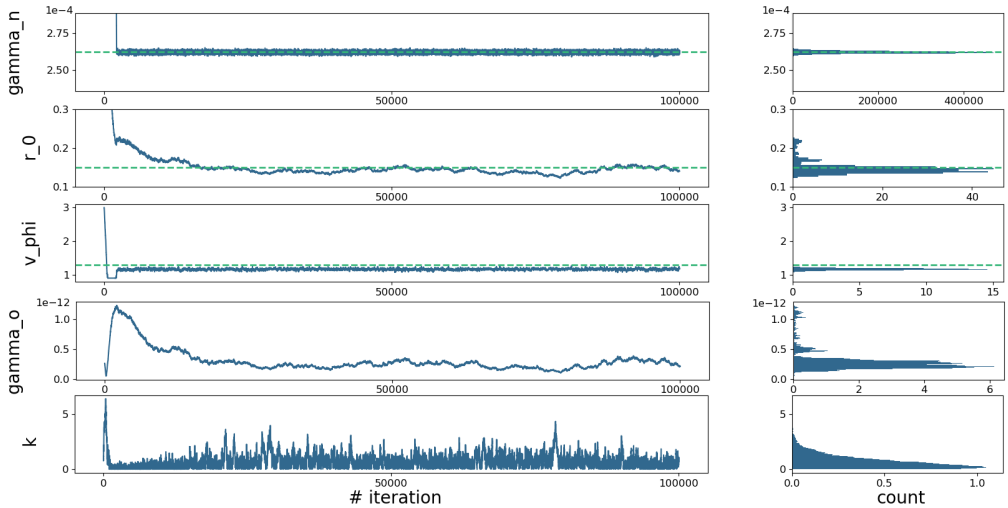

Figure 2. From top to bottom: γ_n, r_0, v_ϕ, γ_o, k. Left: chain of samples for simulated astronomical image. Right: corresponding histogram. True values in dashed line.

The sample mean values m, corresponding to our estimates, and standard deviations σ, corresponding to our predicted uncertainties, for each parameter are displayed in Table 1. Firstly, we can note that the error on the

Parameter	$m \pm \sigma$	True
γ_n (ph^{-2})	$2.620\times10^{-4} \pm 0.008 \times10^{-4}$	2.621×10^{-4}
r_0 (m)	0.142 ± 0.007	0.15
v_ϕ(rad^2)	1.17 ± 0.03	1.30
γ_o (ph^{-2})	$2.37\times10^{-13} \pm 5.41\times10^{-14}$	-
k	0.768 ± 0.594	-

Table 1. Mean value, associated standard deviation and true value, for γ_n, r_0, v_ϕ, γ_o and k for simulated astronomical image (stationary Gaussian noise), with $p = 3$ and $m_o = m_i$.

parameters is small: the noise precision is very precisely estimated, with an error smaller than 0.2%, and PSF parameters are also well estimated, with a 5% error on r_0 and a 10% error on v_ϕ. Additionally, the estimated r_0 and v_ϕ are very close to the previous results obtained with AMIRAL: for similar conditions,[2] the estimated PSF parameters were $r_0 = 0.142\,\text{m}$ and $v_\phi = 1.13\,\text{rad}^2$ (compared to $r_0 = 0.142\,\text{m}$ and $v_\phi = 1.17\,\text{rad}^2$ in Table 1).

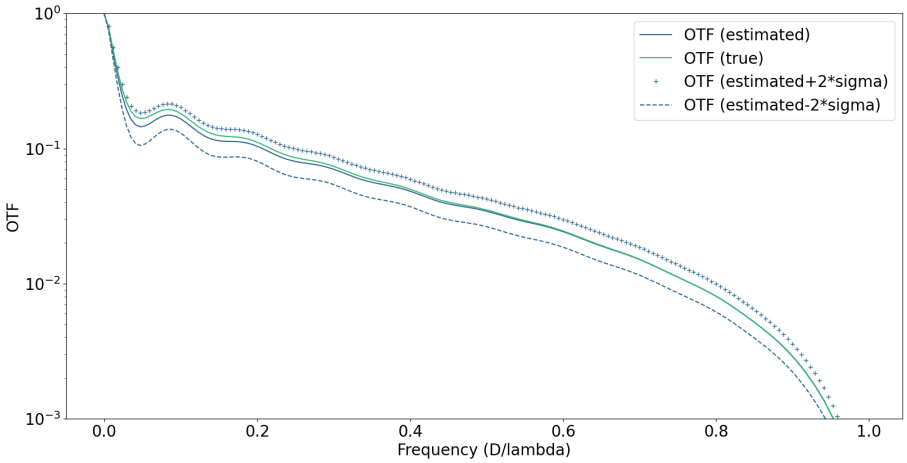

Figure 3. True (in green) and estimated (in blue) OTF for simulated astronomical image, including computed uncertainties (in blue, + and - for upper and lower uncertainty bounds).

3.3 Results on the OTF

We also compare the resulting OTF to the true OTF in Figure 3. The slight underestimation of r_0 leads to the lowering of the global OTF level and its impact can mainly be seen at low frequencies. Concerning v_ϕ, its mild underestimation leads to a slower decrease of the OTF and impacts the slope of the latter at medium-high frequencies.[2] Thus, we notice that the errors on both parameters partially compensate. As a result, the normalized RMSE for the OTFis quite small (around 7%).

Concerning the uncertainties derived from our method, we notice in Table 1 that the true value for parameter r_0 is in the range $[m_{r_0} \pm 2\sigma_{r_0}]$, and the true v_ϕ is in the interval $[m_{v_\phi} \pm 5\sigma_{v_\phi}]$, therefore the uncertainties on PSF parameters seem under-estimated. We can also compute uncertainties directly on the sought OTF: for each sample (r_0, v_ϕ), we compute the corresponding OTF in order to compute its sample mean $m_{\tilde{h}}$ and standard deviation $\sigma_{\tilde{h}}$, meaning the mean and standard deviation for each frequency of the OTF. As shown in Figure 3, the true OTF is within the interval $[m_{\tilde{h}} \pm 2\sigma_{\tilde{h}}]$, for all frequencies. Therefore, even though the uncertainties on PSF parameters are somewhat under-estimated, our method gives a very satisfactory uncertainty estimation on the OTF itself.

3.4 Results on the restored image

Figure 4 shows the image in Figure 1 restored with the estimated OTF, using a quadratic regularization (which hyperparameters are the ones estimated by the method) with positivity constraint. Many details of the Vesta surface can be seen, that were not visible on the data. Particularly, with our method we retrieve sharp edges of

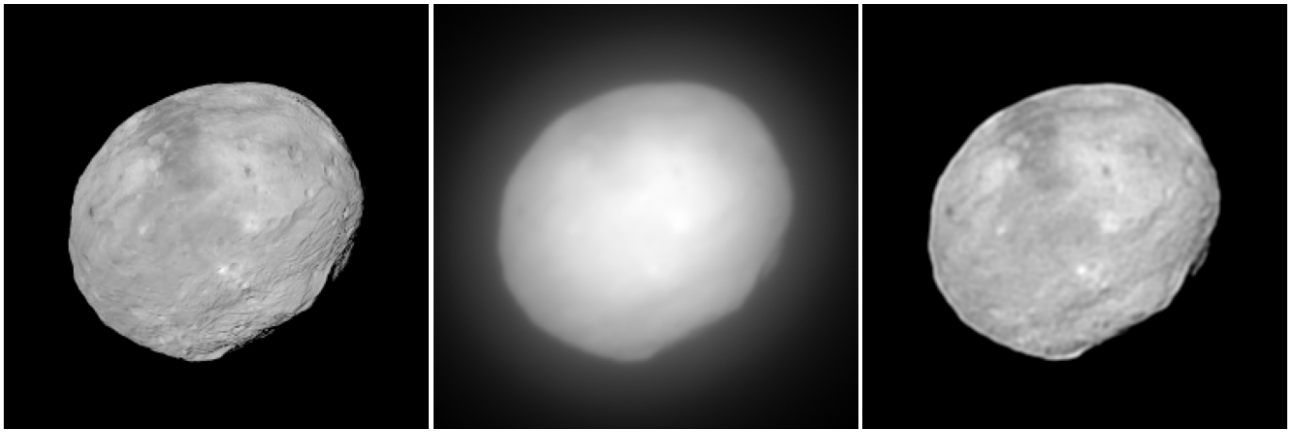

Figure 4. Left and center: true object and image for simulated asteroid observation, 256×256 cropped from Figure 1. Right: restored object from the estimated PSF and PSD parameters using a L2-norm regularization, with positivity constraint, also cropped.

the asteroid from which one can estimate the object volume and sphericity, as well as main crater and albedo features.

3.5 Posterior coupling between parameters

Sampling the whole posterior distribution, instead of computing a single point of it (for example, the maximum), enables us to study the *a posteriori* coupling of the parameters. In Figures 5 and 6, we display the scatter graph of the samples, after boiling time, for two different couples of parameters: (r_0, v_ϕ) and (r_0, γ_o). Most couples of parameters have a scatter graph similar to Figure 5, where the 2D-histogram is rather Gaussian and along the axis suggesting that most parameters are not correlated *a posteriori*.

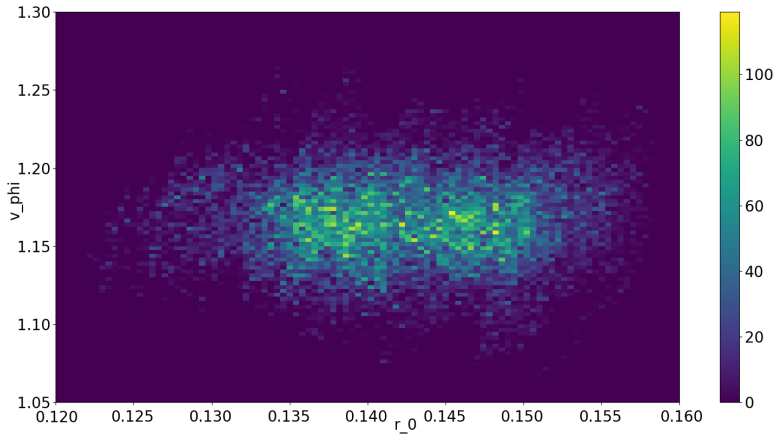

Figure 5. Marginal posterior scatter graph of the samples for (r_0, v_ϕ) after boiling time.

The only couple of parameters which does not have an elliptical-like scatter graph, but instead show a strong *a posteriori* correlation, is r_0 and γ_o. We explain this correlation by the fact that as shown in [2], r_0 impacts the global level of the OTF whereas γ_o gives the global level of the object PSD. Therefore, given the expression of the image PSD in Eq. (5), both (r_0, γ_o) have a similar impact on the global level of the image PSD, which is fitted by our method, that explains their strong correlation.

Additional information and studies (on several noise realizations, with different tunings of hyperparameter p, more realistic noise simulations,...) on this new method are provided in [4].

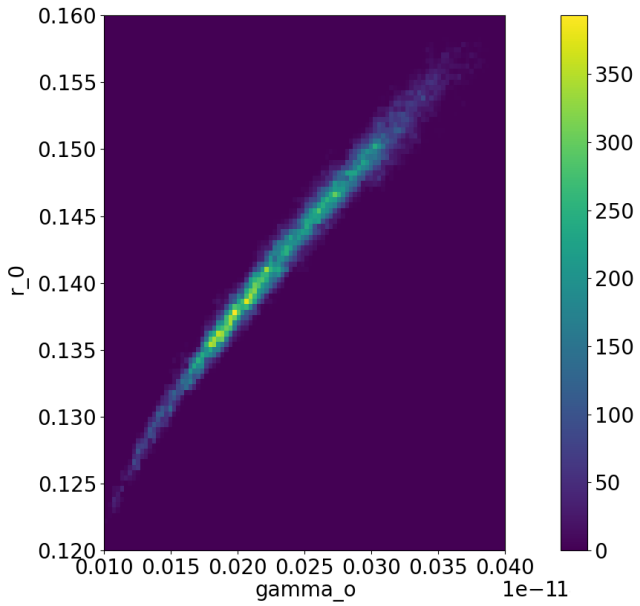

Figure 6. Marginal posterior scatter graph of the samples for (r_0, γ_o) after boiling time.

4. RESULTS ON EXPERIMENTAL ASTRONOMICAL DATA

After testing our method on both astronomical and satellite simulated data, therefore for different turbulence conditions and AO systems, we apply it to experimental images. Here we process an experimental image of Vesta[10] taken by SPHERE/Zimpol in the same mostly unsupervised mode as previously where $p = 3$, and run the Gibbs sampler for 100 000 iterations. Data and restored object are shown in Figure 7. We recognize the same surface features as from the synthetic view in Figure 1. In this experimental case, the bright edge corona starts to appear (on the left side), and the image is slightly granular. This may be due to a slight over-deconvolution *i.e.* to a slight under-estimation of the OTF, as to the quadratic regularization.

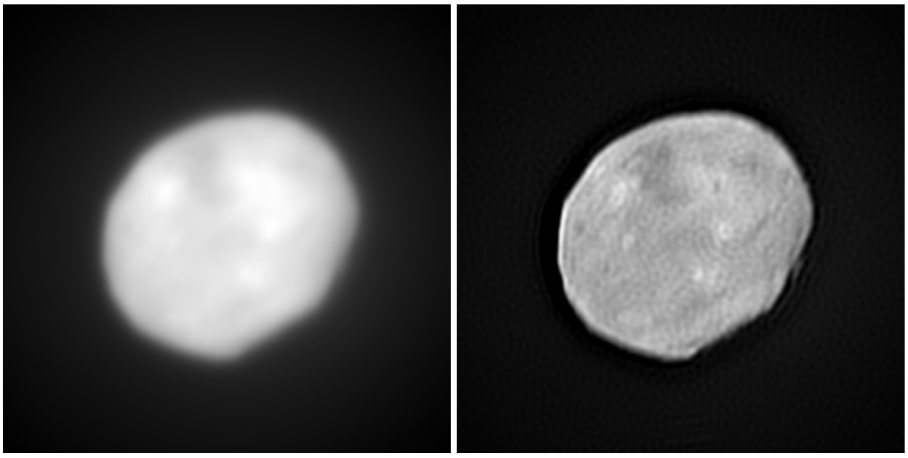

Figure 7. Left: Vesta observed by SPHERE/Zimpol on the European Very Large Telescope (VLT) in Chile.[10] Right: restored object with the estimated PSF using a L2-norm regularization, with positivity constraint.

Results obtained for the PSF parameters (mean±standard deviation) are the following: $r_0 = 0.26 \pm 0.04\,\mathrm{m}$ and $v_\phi = 2.62 \pm 0.06\,\mathrm{rad}^2$. These values are close to the values obtained with AMIRAL[2] ($r_0 = 0.32\,\mathrm{m}$, $v_\phi = 2.78\,\mathrm{rad}^2$) for the same conditions, the newly estimated r_0 being more likely than the one estimated by AMIRAL according to the known statistics on r_0.[6]

5. CONCLUSION

We have presented a new marginal semi-blind deconvolution method extending previous works, using a MCMC algorithm, more precisely a Metropolis-Hastings-within-Gibbs algorithm. In addition to PSF and hyperparameter estimation combined with image restoration, we now have access to the whole posterior distribution. This enables us to compute the optimal estimator minimizing the mean square error. Additionally, with the posterior distribution, we can compute uncertainties based on the posterior standard deviation, as well as posterior correlation between the parameters. This method has been validated on simulated images, giving accurate estimations of noise and object hyperparameters, as well as satisfactory OTF estimations. Finally, our method has also been applied to an experimental image.

In this work, hyperparameter p, which codes for the decrease of the object PSD, has been fixed to a reasonable value according to the class of the object. The PSF estimation quality is sensitive to the choice of p, as we verified it by changing its value.[4] Moreover, jointly estimating p with the other parameters is difficult as mentioned in earlier studies.[2] In the near future, we plan to tackle the joint estimation of p. In order to enable it, and to improve the PSF estimation quality, we are currently working on the addition a support constraint on the object. Indeed, such constraint helps separate the contributions of the object and of the PSF to the image.[11] First results using a support constraint are shown in [12].

Acknowledgements

This study has been partly funded by the French Aerospace Lab (ONERA) in the framework of the SUSA Project. It was also supported by Action Specifique ASHRA of CNRS-INSU co-funded by CNES.

REFERENCES

[1] L. Blanco and L. M. Mugnier, "Marginal blind deconvolution of adaptive optics retinal images," *Optics Express* **19**, 23227 – 23239 (2011).

[2] R. J.-L. Fétick, L. M. Mugnier, T. Fusco, *et al.*, "Blind deconvolution in astronomy with adaptive optics: the parametric marginal approach," *MNRAS* **496**, 4209 – 4220 (2020).

[3] F. Orieux, J.-F. Giovannelli, T. Rodet, *et al.*, "Estimating hyperparameters and instrument parameters in regularized inversion. Illustration for Herschel/SPIRE map making," *Astronomy & Astrophysics* **549**, A83 (2013).

[4] A. Yan, L. M. Mugnier, J.-F. Giovannelli, *et al.*, "Marginalized myopic deconvolution of Adaptive Optics corrected images using MCMC methods," *JATIS (to appear)* (2023).

[5] J.-L. Beuzit, A. Vigan, D. Mouillet, *et al.*, "SPHERE: the exoplanet imager for the very large telescope," *Astronomy & Astrophysics* **631**, A155 (2019).

[6] R. J. L. Fétick, T. Fusco, B. Neichel, *et al.*, "Physics-based model of the adaptive-optics-corrected point spread function," *Astronomy & Astrophysics* **628**, A99 (2019).

[7] J.-M. Conan, L. M. Mugnier, T. Fusco, *et al.*, "Myopic deconvolution of adaptive optics images by use of object and point-spread function power spectra," *Appl. Opt.* **37**, 4614–4622 (1998).

[8] C. P. Robert and G. Casella, *Monte Carlo statistical methods*, vol. 2, Springer (2004).

[9] L. Jorda, S. Spjuth, H. Keller, *et al.*, "OASIS: a simulator to prepare and interpret remote imaging of solar system bodies," in *Computational Imaging VIII*, **7533**, 753311, SPIE (2010).

[10] R. J. Fétick, L. Jorda, P. Vernazza, *et al.*, "Closing the gap between Earth-based and interplanetary mission observations: Vesta seen by VLT/SPHERE," *Astronomy & Astrophysics* **623**, A6 (2019).

[11] C. Vacar, J.-F. Giovannelli, and Y. Berthoumieu, "Bayesian texture classification from indirect observations using fast sampling," *IEEE Transactions on Signal Processing* **64**(1), 146–159 (2016).

[12] A. Yan, *Adaptive-Optics-corrected image restoration for astronomical and satellite observation: marginal approach by stochastic sampling.* PhD thesis, ED127 (2023).